Assesing Fe_3O_4 nanoparticle size by DLS, XRD and AFM

D. CHICEA, E. INDREA[a], C. M. CRETU[b]
Physics Dept., University Lucian Blaga of Sibiu, Dr. Ion Ratiu Str. 7-9, Sibiu, 550012, Romania
[a]*National Institute for Research and Development for Isotopic and Molecular Technologies, Cluj-Napoca, Romania*
Chemistry Dept., University Lucian Blaga of Sibiu
[b]*Chemistry Dept., University Lucian Blaga of Sibiu, Dr. Ion Ratiu Str. 7-9, Sibiu, 550012, Romania*

A simple recipe for preparing a small quantity of magnetite nanaoparticles in aqueous suspension by coprecipitation is presented. The nanoparticles were characterized by X Ray Diffraction, by a nontypical Dynamic Light Scattering procedure and by Atomic Force Microscopy and the results are compared and discussed. The time variation of the refractive index of the aqueous nanofluid during aqueous dilution is presented and discussed in connection with aggregate formation.

(Received January 30, 2012; accepted June 6, 2012)

Keywords: Fe_3O_4 Nanoparticles, X-ray diffraction, Dynamic Light Scattering, Atomic Force Microscopy

1. Introduction

Choi, in 1995 [1] mentioned the nanofluid as a suspension containing a small amount of nanoparticles. The heat transfer properties of a fluid were significantly enhanced by the addition of nanoparticles [2]. The nanoparticles can exhibit novel electronic, magnetic, chemical and optical properties [3–5].

As the nanoparticles are considerably smaller that the living cell or parts of the cells, nanoparticle structured materials are used to investigate, to modify living cells or to deliver certain substances or drugs to them without perturbing much the cells. Many applications of nanostructured materials in biology and medicine were developed in the last years and are presented in review papers, [6] being just one of them.

The physical properties of the nanoparticles and of the nanofluids strongly depend of the size and size distribution, therefore controlling the synthesis and characterizing the samples after synthesis are crucial. The Transmission Electron Microscopy (TEM) is currently used in characterizing nanoparticles and nanometer to micrometer sized clusters. TEM offers the best resolution, but the samples require specific preparation, which makes it expensive and time consuming.

A convenient approach for nanoparticle sizing relays on optical methods involving a coherent light scattering experiment. The target is the suspension, the far field is recorded and a speckle image is otained. The speckled image appears as a result of the interference of the wavelets scattered by the scattering centers (SC hereafter). The image is not static but changes in time as a consequence of the scattering centers complex movement of sedimentation and Brownian motion [7, 8]. Reference [9] reveals that the correlation function of the near-field speckle depends of the particles size. The work reported in [10] and [11] uses a transmission optical set-up to measure the far field parameters like contrast and speckle size and reveals that speckle size and contrast are related to the average particle diameter. Ref. [12] revealed a strong variation of the average speckle size and contrast with the concentration of the scattering centers, but the work described here deals with samples that can have both different nanoparticle concentration and size, therefore the speckle analysis technique is not suited for particle sizing.

The speckle dynamics is closely related to the Brownian motion of the nanoparticles. The physical method that exploits this correlation is called Dynamic Light Scattering (DLS) or Photon Correlation Spectroscopy (PCS) and the physical principles of the method are explained in [7 - 9] and in many other papers following them. A nontypical DLS setup and data processing was used in the work reported here to assess the average nanoparticle size and is briefly described in the dedicated section of this paper.

Another physical method involving coherent light scattering currently used to measure the average nanoparticle size in suspension is the modified version of the Static Light Scattering (SLS) experiment. The light scattering anisotropy coefficient *g* strongly depends of the scattering center diameter. A functional dependence of the g parameter with the nanoparticle diameter can be derived using Mie calculations. Once the g parameter is assessed using a least square fit, the average diameter can be derived using the functional dependence calculated for that particular type of nanoparticles, as described in [13], [14].

Another physical procedure that can be used to assess the nanoparticle size is the Atomic Force Microscopy (AFM). Some of the papers that report using AFM for nanoparticle sizing are [15] and [16]. A comparison of the TEM with the AFM results is presented in [17]. The AFM technique and the results using it are presented in the dedicated section of this paper.

The X-ray powder diffraction is just another technique currently used in assessing the nanoparticle diameter [18]. Moreover, the areas under the peak are related to the

amount of each phase present in the sample. The Scherrer equation [19] is frequently used in X-Ray analysis, particularly powder diffraction. It relates the peak full width at half maximum of a specific phase of a material to the mean crystallite size of that material, assuming that the nanoparticle size is the same as the size of the crystallite.

The following sections describe the recipe used in preparing a small amount of Fe_3O_4 nanoparticles in aqueous suspension, the results of the X Ray Diffraction, DLS and AFM characterization. The time variation of the refractive index after aqueous dilution is presented as well.

2. Nanofluid synthesis recipe

The procedure we used to prepare the aqueous nanofluid is a typical coprecipitation. The reagents used were: $FeCl_2 \cdot 4H_2O$, $FeCl_3 \cdot 6H2O$, ammonium hydroxide (NH_3[aq]), citric acid ($C_6H_8O_7$), all produced by Merck, Darmstadt. Double deionised water was used to dissolve the reagents.

The solutions were prepared right before synthesis, in order to prevent their contamination with atmospheric oxygen. First 10.44g of $FeCl_3 \cdot 6H2O$ and 4.16 g of $FeCl_2 \cdot 4H_2O$, were dissolved in 0.380 l of double deionised water. The temperature was risen at 75°C and maintained at this value while continuously stirring the solution. 40 ml of 25% ammonium hydroxide were slowly added, one drop at a time, in such a manner that the addition process lasted for 30 minutes. A black precipitate was formed during the slow addition, the precipitate being magnetite ($Fe^{2+}Fe^{3+}{}_2O_4$). A strong magnet was placed under the beaker. It pulled all of the magnetite out of the solution, and the water become clear. While maintaining the magnet on the bottom of the beaker, the excess water was discarded.

The magnetite was rinsed three times by adding deionised water at 50 °C, using the magnet to settle the magnetite, and discarding the clear water, to completely remove the excess ammonium hydroxide from the particles. At the end of this stage of the preparation process the solution pH was 7.5.

At this stage of the synthesis procedure the nanofluid must be stabilized. Stabilization was accomplished by adding 1 mL of the 42% citric acid and mixing the ferrofluid for 2 minutes by moving the beaker over the magnet and keeping the temperature at 80°C.

Overall the chemical reaction was:

$$2FeCl_3 + FeCl_2 + 8NH_3 + 4H_2O \rightarrow Fe_3O_4 + 8NH_4Cl \quad (1)$$

Again excess solution was discarded. The output was a viscous, black fluid. The volume fraction ϕ of nanoparticle phase in the nanofluid sample was calculated using mass density measurements using Eq. (2):

$$\varphi = \frac{\rho_f - \rho_l}{\rho_s - \rho_l} \quad (2)$$

where ρ_f is the density of the ferrofluid, ρ_l the density of the carrier fluid and ρ_s the density of the solid particles. Density was measured using a picnometer at T = 293K. Using (2) we found that the volume fraction ϕ of nanoparticles was 8.23%. The nanofluid obtained using this procedure remained stable for 16 month that passed since producing it till writing the manuscript of this article.

The recipe and the procedure used in manufacturing the nanofluid are different from the simple procedure reported in [20] as the temperature was not maintained constant at 20°C but was carefully monitored, controlled and maintained at 75°C during the co-precipitation stage of the synthesis. The purpose of the change was to favor magnetite formation and to prevent maghemite formation at lower temperatures. The nanofluid produced in the work reported in [20] had brown and red reflexes, indicating the presence of maghemite. Reference [21] using TEM reports that by using a temperature range of 65-75 ^{0}C, the procedure will produce spherical magnetite nanoparticles. References [22] and [23] reveal the influence of the temperature on the shape and size distribution of the nanoparticles produced by coprecipitation.

The nanofluid we obtained was clearly black with no red or brown reflexes, meaning that the nanoparticles were magnetite (Fe_3O_4) not maghemite (γ-Fe_2O_3).

The following section describes the X ray power diffraction procedure used for investigating the nanoparticle size distribution.

3. X ray powder diffraction characterization

In order to perform an Xray powder diffraction experiment, the sample has to be brought to powder phase. This was accomplished by maintaining 0.5 ml of the liquid sample as described in the previous section to 85 °C for 2 hours, till it became a black solid sample. It was removed from the bottom of the Petri dish with the blade of a cutter and deposited in the sample holder of the X ray diffractometer.

The powder X-ray diffraction (XRD) patterns were obtained with a Bruker D8 Advance powder diffractometer working at 40 kV and 40mA, using CuKα wavelength, with a Germanium monochromator. The measurement was performed in the range angle 2θ=15-85^0 and in a step-scanning mode with a step $\Delta 2\theta = 0.01^0$. Pure corundum powder standard sample was used to correct the data for instrumental broadening.

The XRD patterns of the investigated samples were used for crystal phase analysis. Phase analysis was carried out using the unit cell parameters calculated through structure refinement using the PowderCell software [24].

The microstructural information obtained by single X-ray profile Fourier analysis of the magnetite Fe_3O_4 - cubic crystalline phase were the effective crystallite mean size, D_{eff} (nm) and the root mean square (rms) of the microstrains, $\langle\varepsilon^2\rangle^{1/2}_m$, [25], [26]. The Warren-Averbach X-ray Fourier analysis peak profiles were processed by the XRLINE computer program [27].

The XRD diffraction pattern, presented in Fig.1, illustrates the fact that the sample obtained in our synthesis conditions is magnetite Fe_3O_4 – cubic crystalline structure phase [28].

The Warren-Averbach X-ray Fourier analysis of the (311) and (333) cubic magnetite Fe_3O_4 diffraction profiles was carried on in order to determine the microstructural parameters of the magnetite Fe_3O_4 - cubic crystalline phase. The values we found are presented in Table 1 and illustrated in Figs. 2 and 3.

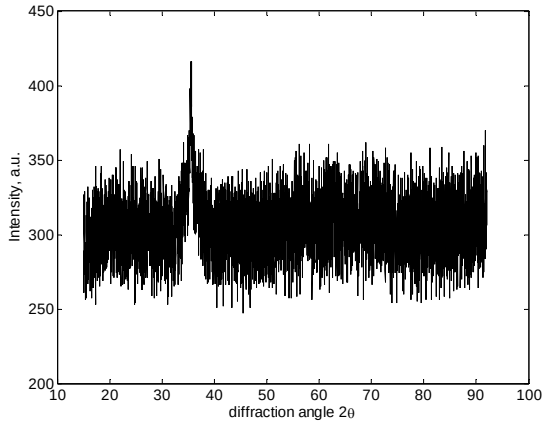

Fig 1. X-ray diffraction pattern for the analyzed sample with the magnetite Fe_3O_4 - cubic crystalline structure phase.

Table 1. Unit cell dimensions and microstructural parameters for the magnetite sample

Sample	a=b=c, [nm]	V [nm^3]	D,[nm]	$\langle\varepsilon^2\rangle^{1/2}$ x 10^3
magnetite	0.8366(8)	0.5857(1)	10.9	2.153

The crystallite size distribution function was determined from the second derivative of the strain corrected Fourier coefficients [27]. The effective crystallite mean size distribution function D(L) for the magnetite sample reveals a broad distribution of the crystallites dimensions around 11 nm mean value, as revealed by Fig. 2.

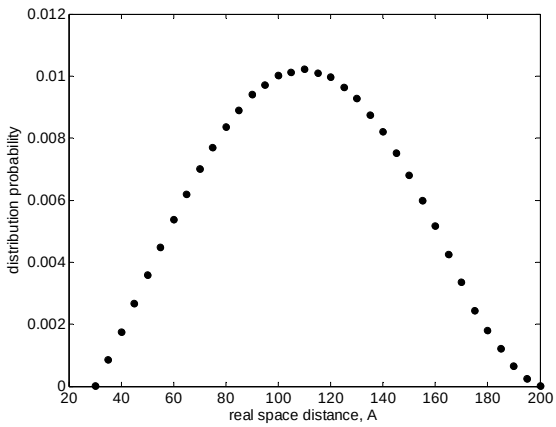

Fig. 2. Effective crystallite size distribution function D(L) for magnetite Fe_3O_4 nanostructure

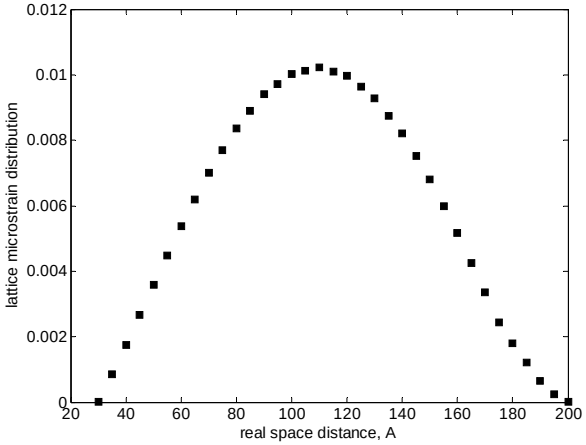

Fig. 3. Lattice microstrain distribution for the magnetite Fe_3O_4 nanostructure

The lattice microstrain distribution function $\langle\varepsilon^2\rangle^{1/2}(L)$ for the magnetite sample, Fig. 3, presents an increased value in the intercrystallite zones with a large amount of crystalline lattice defects, which suggest a higher chemical reactivity at the surface of the crystallites in this sample. The root mean square of the lattice microstrain distribution $\langle\varepsilon^2\rangle^{1/2}$ for the magnetite Fe_3O_4 nanostructure was found to be $2.153 \cdot 10^{-3}$. The results of the powder diffraction experiment are consistent with the results reported in the literature on Fe_3O_4 nanoparticles, [29] being just one of them.

4. Nanoparticle sizing by DLS

The Dynamic Light Scattering (DLS) is a technique currently used for measuring particle size over a size range from nanometers to microns. The light scattered by a suspension presents fluctuations, [7, 8]. By placing a detector at a certain angle and recording the scattered light intensity a time series is recorded. The width of the autocorrelation function of the time series is proportional to the diffusion coefficient, which, on its turn, depends of the particle diameter [30], [31]. This leads to a fast procedure for measuring the particle diameter.

Former and recent theoretical work [32-34] proved that the power spectrum of the intensity of the light scattered by particles in suspension is linked to the probability density function (hereafter PDF). This link between the PDF and the power spectrum is a consequence of the translation of the relative motion of the scattering particles into phase differences of the scattered light. The spatial correlations are therefore translated into phase correlations. According to the Wiener-Khintchine-Theorem, this translation relates the power spectrum to the autocorrelation function of a process. The phase correlations lead to fluctuations of the intensity of the scattered light recorded using a detector and a data acquisition system, in a typical experimental setup, as presented in Fig. 4.

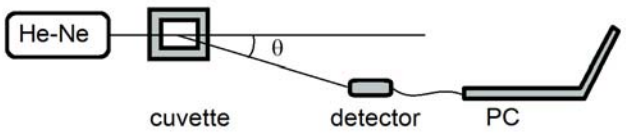

Fig. 4. A typical DLS experimental setup, view from above.

By subtracting the average intensity from the recorded time series and calculating the square of the intensity we obtain the power time series. The Fourier transform of the power time series is the power spectrum. We can compare the spectrum calculated from the experimental data with the theoretically expected spectrum, namely the functional form of the Lorentzian line S(f), described by Eq. (3).

$$S(f) = a_0 \cdot \frac{a_1}{(2\pi f)^2 + a_1^2} \tag{3}$$

The Lorentzian line S(f) has two parameters a_0 and a_1 and is fit to the power spectrum using a non-linear minimization procedure. Eq. (3) reveals that a_0 enters linearly, thus only performing a scaling of the function in the range, which translates into a shift in the logarithmic representation. The a_1 parameter enters nonlinearly into the function. Its effect in the loglog scaled plot can approximately be described as a shift along the frequency axis. The possibility to fit the whole function is advantageous compared to the alternative method described in Refs. [8] where the $f_{1/2}$ (the frequency where half-maximal-height is reached) was measured, since it takes more data points into account, therefore increasing the quality of the fit.

Once the fit is completed and the parameters are found, the diameter of the SCs can be assessed as the double of the radius R. The radius can be derived as a function of the fitted parameter a_1 and other known quantities using (3):

$$R = \frac{2k_B T K^2}{6\pi\eta a_1} \tag{4}$$

Where:

$$K = \frac{4\pi n}{\lambda} \cdot \sin\left(\frac{\theta}{2}\right) \tag{5}$$

In (4) k_B is Boltzman's constant, T is the absolute temperature of the sample, η is the dynamic viscosity of the solvent. In (5) θ is the scattering angle, n is the refractive index of the scattering particles and λ is the wavelength of the laser radiation in vacuum.

The work described in this article was carried on using an experimental setup as presented in Fig. 4. The wavelength was 633 nm, the light source was a He-Ne laser and the power was 2 mW, working in a continuous regime. The DLS experiment was carried on at 22 ^oC. The cuvette-detector distance D was 0.41 m and x was 0.0225 m making the scattering angle θ equal to 3^o 8' 28''. This is not typical for DLS where a bigger angle is chosen, usually 90^o. The reason for choosing such a small angle is to shift the rollover point in the Lorentzian line towards smaller a_1 values, hence smaller frequencies, where the noise is considerably smaller.

The concentrated nanoparticle suspension was diluted in 15 % citric acid, in order to prevent aggregation. Nanoparticles aggregation in diluted aqueous suspension is a very fast process, as presented in Refs. [13], [14] and [35]. A DLS time series was recorded. The time series was analysed using the procedure described above. The PSD (scattered line) and the fitted Lorentzian (smooth line) for the time series recorded on sample are presented in Fig. 5. The PSD plot reveals that the acquisition rate used in this work is bigger than in previous work [14] and [35]. The acquisition rate was 1250 Hz, as compared to 100 Hz in [35]. This increases the amount of data to be fit to, reducing the data acquisition time, reducing the probability of recording fluctuations caused by electric power grid perturbations and therefore increasing the precision of the fit.

The parameters of the Lorentzian line found from the fit are: a_0=51.99and a_1=52.14. Using (4) and (5) we found that the SCs have an average diameter of $12 \cdot 10^{-9}$ m. At this point we have to mention that a commercial DLS particle analyzer uses more than one array of detectors placed at several angles rather than one detector and the backscattered light is used for measuring particle size in the nanometer range. The one detector, forward scattering DLS setup and the data processing used in this work is the same as the one used in [35] for monitoring nanoparticle aggregation, except for the data acquisition system and is less sensitive in the nanoparticle size range. With these facts in mind we must state that the error in assessing the particle diameter in the nanometer range using this setup is considerably big, rising up to 80%. Nevertheless, this result is consistent with the Xray powder diffraction, considering the unavoidable experimental errors.

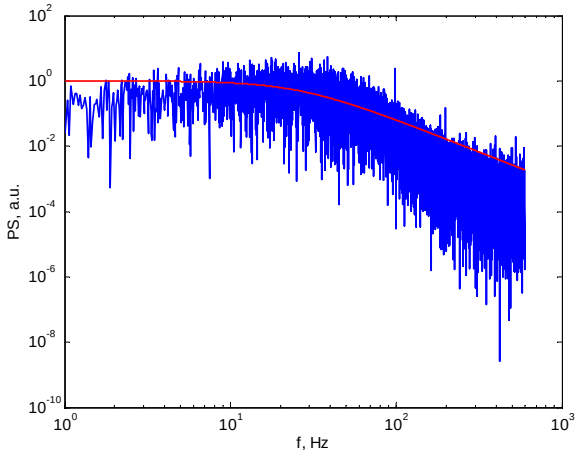

Fig. 5. The PSD (scattered) and the fitted Lorentzian line (smooth) for the time series recorded on nanofluid diluted in citric acid to prevent aggregation.

The next section describes the AFM characterization of the nanoparticles.

5. AFM measurements

The atomic force microscope (AFM) is a scanning probe microscope. The AFM uses a flexible cantilever to measure the force between the tip and the sample. The basic idea of an AFM is that the local attractive or repulsive force between the tip and the sample is translated into a deflection of the cantilever. The cantilever is attached to a rigid substrate that can be held fixed, and depending whether the interaction at the tip is attractive or repulsive, the cantilever will deflect towards or away from the surface [36].

The detection system uses a laser beam that is reflected from the back of the cantilever onto a detector. The optical lever principle is used. This states that a small change in the bending angle of the cantilever is converted to a precisely measurable deflection in the position of the reflected spot. By scanning the sample line by line and using a calibration file for each mode of operation and cantilever type a topography image of the surface is reconstructed by the software that drives the scanning process.

The AFM that was used in the work reported here is an Agilent 5500 type. The scanning mode was ACAFM. A soft tip, having the spring constant equal to 5 N/m was used at low force amplitude. As the nanoparticles or nanoparticle aggregates undergo a Brownian motion in suspension, scanning in liquid can not be used for nanoparticle sizing.

Sample preparation is crucial in order to get useful AFM images [16]. Samples must be thin enough and must adhere well to the surface, otherwise the scanning process will producing artefacts. More details are presented in [16] and [37].

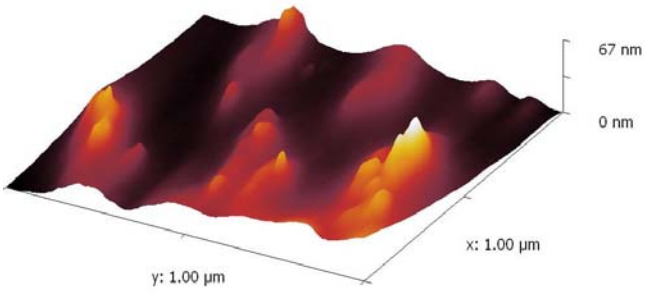

Fig. 6 The 3D topography of the evaporated nanofluid deposited on a freshly cleaved mica surface. Z axis is in nm.

In order to prepare the sample a drop of nanofluid was deposited on a freshly cleaved mica substrate and stretched with blade to form a very thin layer. The thin layer was left for 3 hours to evaporate. The sample was attached to the AFM plate. First a large area (5 µm x 5 µm) surface scan was carried on.

As the resolution used in the first scan is not good enough to image nanoparticles on a surface, several scans were carried on selecting a flat area on the surface where there appears to be singular nanoparticles rather than aggregates, which were present, as well. Finally, a bigger resolution scan, (512x512 pixels) was achieved and the topography is presented in Fig. 6. The scanned area is 1.0 µm x 1.0 µm.

Examining Fig. 6 we notice several nanoparticles located on the scanned area. Three nanoparticles appear to be aligned in the bottom right part of the image.

The 3D topography images are not the best way to assess nanoparticles dimension, but profiles extracted from the images can produce accurate information. Fig. 7 presents several profiles extracted over nanoparticles, one of them being across the three aligned nanoparticles in the bottom right corner.

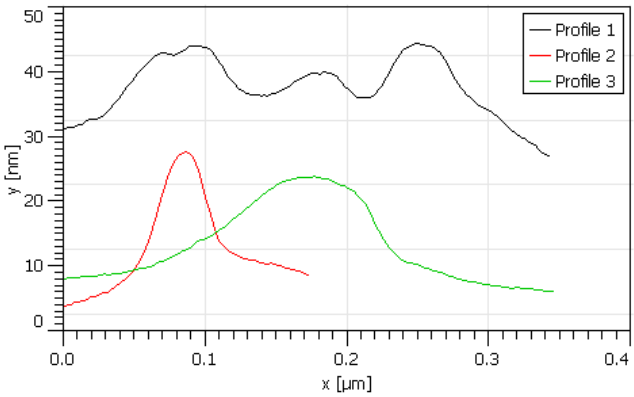

Fig. 7 Profiles extracted over nanoparticles

The difference between the top and the base line values of the curves indicate the size of the nanoparticle. Examining the profiles in Fig. 7 we notice that the size of the nanoparticles is around 11 – 15 nm, which is consistent with the DLS nanoparticle sizing experiment results presented in the previous section and with effective crystallite mean size assessed by XRD, as presented in section 3.

6. Refractive index measurements

A concentrated Fe_3O_4 nanofluid is opaque, therefore a smaller concentration nanofluid was prepared to conduct a refractive index measurement. The refractometer was a DRC-200 Abbe type digital refractometer and was placed in a setup to produce one measurement every 0.9 s. The resolution of the refractometer is 0.0001. The refractometer display was optically recorded during the experiment and the refractive index variation in time was extracted later on.

The temperature of the environment where the measurements were carried on was 23.4 ^{o}C. Very small amounts of solvent and nanofluid were used: 0.4 ml of deionized water and 0.02 ml of nanofluid, prepared as

described in section 2 of this paper. First the deionized water was placed in the open sample location of the refractometer. The small amount of nanofluid was first aspired in a 1 ml syringe and injected in the deionized water already placed into the refractometer. Recording was started 5 seconds prior of nanofluid injection and this constant, flat part prior of nanofluid injection is not presented in Fig. 8, which presents the time variation of the refractive index during nanofluid dilution in deionized water, starting with the beginning of the dilution assigned to t=0s.

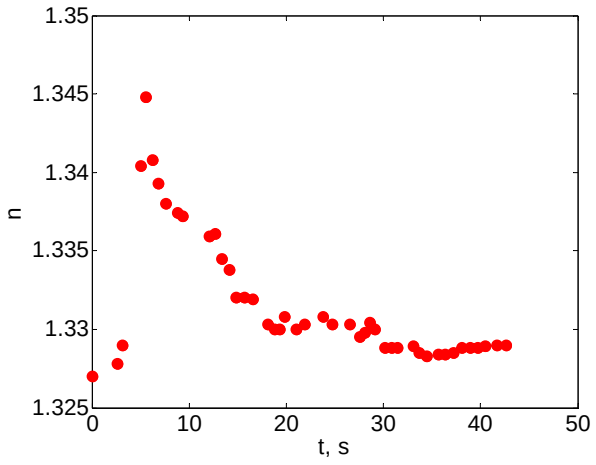

Fig. 8 The time variation of the refractive index of the diluted nanofluid.

Fig. 8 reveals a fast increase of the refractive index during the first 4 seconds of the dilution process. This time interval is consistent with the time required for the diluted nanofluid to get homogenized by the convection currents produced by injection. The refractive index of the diluted nanofluid is slightly bigger than the index of the deionized water, because the suspension, the ferrite nanoparticles, has a bigger refractive index, around 1.6, typical for glassy substances.

As time passes, a fast aggregation occurs in the diluted aqueous nanofluid, as presented in [13], [14], [35]. The number of aggregates is much smaller than the number of nanoparticles and this explains the decrease in the refractive index of the diluted nanofluid. The decrease lasted for about 30 s and this time interval is consistent with the aggregation time reported in [13], [14], [35]. The aggregation time depends both of the temperature and of the geometry of the vessel where the process carries on, therefore time differences of several seconds are quite normal. Nevertheless, the final refractive index of the diluted nanofluid is 1.3290, slightly bigger than 1.3270 that was measured for the deionized water sample used for dilution.

7. Discussions and conclusion

The three methods used in assessing the nanoparticle dimension, The X Rays Diffraction, the Dynamic Light Scattering and the Atomic Force Microscopy are essentially different.

The XRD diffraction pattern illustrates that the sample obtained in our synthesis conditions is magnetite Fe_3O_4 - cubic crystalline structure phase. The Warren-Averbach X-ray Fourier analysis of the (311) and (333) cubic magnetite Fe_3O_4 diffraction profiles was used to determine the microstructural parameters of Fe_3O_4 - cubic crystalline phase, which are the effective crystallite mean size, D_{eff} (nm) and the root mean square (rms) of the microstrains. We found that the crystallite mean size was 10.9 nm. This method assumes that the effective crystallite mean size is the same as the physical size of the nanoparticles. This assumption is true, unless the nanoparticles aggregate in the solvent and the solvent evaporates during sample preparation after the aggregation process is completed, as described in [13] and [35]. Special care was taken in the sample preparation used in the work described in this article to avoid aggregation, therefore we can assume that the nanoparticle average dimension is the same with the effective crystallite mean size assessed by XRD.

In the DLS technique the width of the autocorrelation function of the time series is proportional to the diffusion coefficient, which, on its turn, depends of the particle diameter. Consequently the measured diameter is not the physical diameter, but the hydrodynamic diameter [35]. Moreover, as light scattering can be approximated as a Rayleight type of scattering, the scattered light intensity is proportional to the 6-th power of the scatterer diameter, as presented in [35], therefore the average diameter derived using the procedure described in section 4 should be considered as an average size of the bigger nanoparticles. The DLS diameter we found was 12 nm. Considering these facts we notice that the DLS result is consistent with the XRD result concerning the nanoparticle diameter.

The AFM technique uses an image reconstruction from successive lines acquired during a scan of the surface. A profile can be extracted form the topography of the surface and the particle dimension can be assessed from the profile. Special care must be taken though, because the cantilever tip has a finite dimension, which is not fully controlled by the technology used in manufacturing them. Moreover, the cantilever is a consumable in the AFM technique, as the tip wears out during scanning, by becoming less sharp, therefore having a bigger tip radius [37]. Even the sharp new tips have a tip diameter around 40 nm and are used to scan details on the order of 10 nm. Further details and the precautions on measuring nanoparticles diameter when using AFM are presented in [16].

The AFM technique produces results on the physical diameter of the nanoparticles attached to a substrate, not the hydrodynamic diameter as the DLS, therefore the differences that occur in the output are natural. Nevertheless, the nanoparticle size determined by AFM is consistent with the results of the DLS and XRD techniques.

The work presented in this article was carried on to characterize the Fe_3O_4 nanofluid prepared using a simple coprecipitation procedure. The results we found using

three different physical methods were found to be comparable, considering the inherent systematic errors, therefore we can conclude that the AFM method is a complementary method to the classical DLS and XRD. Moreover, the AFM can be used to investigate the small size particle distribution "tale", while the DLS is significantly less sensitive for smaller sized nanoparticles if the particles have a wider size distribution. Even more, AFM can be used to create images of the nanoparticles that were made to adhere to an atomic scale plane substrate, thus enabling a nanoparticle shape analysis.

References

[1] U. S. Choi, ASME Fed. **231**, 99 (1995).
[2] P. Vadasz, J. Heat Transfer. **128** 465 (2006).
[3] W.C. Lin, P.C. Huang, K.J. Song, M.T. Lin, Appl. Phys. Lett. **88**(153), 117 (2006)
[4] V.V. Agrawal, G.U. Kulkarni, C.N.R. Rao, J. Phys. Chem. B **109**, 7300 (2005).
[5] A. Babapour, O. Akhavan, R. Azimirad, A. Z. Moshfegh, Nanotechnology **17**, 763 (2006)
[6] O. V. Salata, Journal of Nanobiotechnology, **2,** 3 (2004), doi:10.1186/1477-3155-2-3.
[7] J. W. Goodman, Laser speckle and related phenomena, Vol. 9 in series Topics in Applied Physics, J.C. Dainty, Ed., Springer-Verlag, Berlin, Heidelberg, New York, Tokyo, (1984).
[8] Briers J. D.: Laser Doppler, speckle and related techniques for blood perfusion mapping and imaging, Physiol. Meas. **22,** R35–R66, (2001).
[9] M. Giglio, M. Carpineti, A. Vailati and D. Brogioli, Appl. Opt. **40**, 4036 (2001).
[10] Y. Piederrière, J. Cariou, Y. Guern, B. Le Jeune, G. Le Brun, J. Lotrian, Optics Express **12**, 176, (2004).
[11] Y. Piederriere, J. Le Meur, J. Cariou, J.F. Abgrall, M.T. Blouch, Optics Express **12**, 4596 (2004).
[12] D. Chicea, European Physical Journal Applied Physics **40**, 305 (2007). DOI: 10.1051/epjap:2007163
[13] D. Chicea, J. Optoelectron. Adv. Mater. **12**(1), 152 (2010).
[14] D. Chicea, Current Nanosciene 8, 259-265 (2012).
[15] F. Zhang, S.W. Chan, J. E. Spanier, E. Apak, Q. Jin, R. D. Robinson, I. P. Herman, Appl. Phys. Lett. **80**, 27 (2002); doi:10.1063/1.1430502.
[16] D. Chicea, Optoelectron. Adv. Mater. – Rapid Comm. **4**(9), 1310 (2010).
[17] L. M. Lacava, B. M. Lacava, R. B. Azevedo, Z. G. M. Lacava, N. Buske, A. L. Tronconi, P. C. Morais, Journal of Magnetism and Magnetic Materials, **225**(1-2), 79 (2001).
[18] A. W. Hull, A new method of chemical analysis, J. Am. Chem. Soc., **41**(8), 1168 (1919), doi: 10.1021/ja02229a003
[19] Patterson A. L.: The Scherrer Formula for X-Ray Particle Size Determination Phys. Rev. **56**(10), 978 (1939), doi:10.1103/PhysRev.56.978.
[20] D. Chicea, C. M. Goncea, Optoelectron. Adv. Mater. – Rapid Comm. **3**(3), 185 (2009).
[21] G.F. Goya, T.S. Berquo, F.C. Fonseaca, M.P. Morales, Journal of Applied Physics **94**, 3520 (2003).
[22] Z.L Liu, Y.J. Liu, K.L. Yao, Y.H. Ding, J. Tao, X. Wang, Journal of Materials Synthesis and Processing **10**, 83 (2002).
[23] L.Vayssieres, C. Chaneac, E. Tronc, J.P. Jolinet, Journal of Colloid and Interface Science **205**, 205 (1998).
[24] W. Kraus, G. Nolze, POWDER CELL J. Appl. Crystallogr. **29** 301 (1996**)**.
[25] J.G.M. van Bercum, A.C. Vermeulen, R. Delhez, T.H. de Keijser, E.M. Mittemeijer, J.Appl. Phys., **27,** 345 (1994).
[26] E. Indrea, Adriana Barbu, Appl. Surf. Sci., **106,** 498 (1996).
[27] N. Aldea, E. Indrea, Comput. Phys. Commun., **60**, 155 (1990).
[28] R.T. Downs, M. Hall-Wallace, American Mineralogist, **88**, 247 (2003).
[29] J.Wan, G. Tang, y. Qian, Appl. Phys. A **86**, 261 (2007).
[30] W. Tscharnuter, in Encyclopedia of Analytical Chemistry, R.A. Meyers (ed), John Wiley & Sons Ltd, 5469-5485, (2000).
[31] B. B. Weiner, Chapt. 5 in Liquid-and Surface-Borne Particle Measurement Handbook, J. Z. Knapp, T. A. Barber and A. Liebermann (ed), Marcel Dekker Inc. NY, (1996).
[32] Berne and Pecora, Dynamic Light scattering, John Wiley, (1975).
[33] J.W. Goodman, Statistical Optics, Wiley Classics Library Edition, (2000).
[34] E. Hecht, Optics, Addison-Wesley, New York, 2001.
[35] D. Chicea, Optoelectron. Adv. Mater. – Rapid Comm. **3(**12), 1299 (2009).
[36] http://www.jpk.com/general-scanning-probe-microscopy.431.html
[37] D. Chicea, B. Neamtu, R. Chicea, L. M. Chicea, Digest Journal of Nanomaterials and Biostructures **5(**4), 1015 (2010).

*Corresponding author: dan.chicea@ulbsibiu.ro